JOURNAL OF MATERIALS SCIENCE 22 (1987) 2447–2456

Electron microscopy of second phases in manganese–zinc ferrite crystals

M. J. REECE*, D. J. BARBER
Physics Department, University of Essex, Colchester, Essex CO4 3SQ, UK

The surface and bulk microstructure of Mn–Zn ferrite single crystals oxidized at 0.7% p_{O_2} have been investigated using SEM and TEM methods, assisted by energy-dispersive X-ray microanalysis. In samples heat-treated at 1000° C, haematite formed as an irregular surface layer and as laths which grew throughout the bulk, parallel with the $\{1\,1\,1\}_F$ planes (where F = ferrite). The haematite laths were related epitaxially to the ferrite host through the relationships $(0\,0\,0\,1)_H \parallel \{1\,1\,1\}_F$ (where H = haematite) and $\langle\bar{1}\,0\,1\,0\rangle_H \parallel \langle\bar{1}\,1\,0\rangle_F$. However, it was found that the latter parallelism was not exact because the haematite and ferrite lattices were rotated by 1.1 ± 0.2° about the axis perpendicular to the interface between them (i.e. $[0\,0\,0\,1]_H$, $\langle 1\,1\,1\rangle_F$). The sites for the nucleation of haematite second phase were also observed in highly oxidized ferrite. The formation of small planar defects (< 0.1 μm in length) in the ferrite, lying parallel to $\{1\,1\,0\}$ planes, is interpreted as the combination of a local shear with the ordering of cation vacancies resulting from the oxidation. Small volumes of other second phases were also recognized, by virtue of both compositional and microstructural differences from the host ferrite.

1. Introduction

Manganese zinc ferrites belong to the group of "soft" ferrite materials characterized by high magnetic permeabilities and low losses. Mn–Zn ferrites are the most important soft ferrites because in polycrystalline form they have numerous electronic applications. More recently single crystals have been employed in magnetic recording heads [1, 2]. This has led to an interest in the mechanical and tribological properties of soft ferrites and how these relate to non-stoichiometry and second-phase effects. The results reported below are part of a collaborative investigation and some related results have already been reported [3].

Mn–Zn ferrites have the spinel structure (space group Fd3m) and are usually grown by the Verneuil method, as were those used in this work. Because non-stoichiometry of oxygen easily occurs at high temperatures [4], crystal growth (and any subsequent annealing) must be carried out at a controlled partial pressure of oxygen (p_{O_2}) or in combination with other methods for adjusting the composition [5].

In stoichiometric spinel, 8 of the 64 possible tetrahedral A sites and 16 of the 32 possible octahedral B sites are occupied in the unit cell (see e.g. Greenwood [6]). In Mn–Zn ferrite, the manganese cations are found on both A and B sites [7] which makes it a partially-inverse spinel. Non-stoichiometry, in the form of excess oxygen, produces cation vacancies on both A and B sites as shown by Morineau and Paulus [28] and Morineau [9]. Such non-stoichiometry has considerable effects on electrical properties [10], magnetic properties (see e.g. Ohta [11], Gallagher *et al.* [12]) and mechanical strength (see e.g. Tanaka [13], Kosinski *et al.* [14]).

Ferrites were some of the first bulk non-metals to be ion-thinned and studied by transmission electron microscopy [8]. Subsequently the nature of lattice defects in spinel-structured ferrites was investigated by several research groups (e.g. Baker and Whelan [15], Van der Biest and Thomas [16], Veyssière *et al.* [17, 18]. It was established that the normal dislocation Burgers vector was $(a/2)\langle 1\,1\,0\rangle$ and that growth-induced stacking faults in the cation sublattice occur on $\{1\,1\,0\}$ planes with a displacement vector of $(a/4)\langle 1\,1\,0\rangle$ perpendicular to the plane of the stacking fault.

TEM studies of the interactions between magnetic domain walls and defect microstructure in ferrites and related materials have been reported by Mishra and Thomas [19] and by Lin *et al.* [20], the former giving a useful summary of electron microscopy on ferrites. TEM work has also been carried out by Thomas and co-workers on the non-centrosymmetric ferrite $LiFe_5O_8$ (e.g. Mishra [21], Mishra *et al.* [22]). This material is enantiomorphic and it is the only ferrite reported to exhibit long-range order, although all mixed-cation ferrites could order, in principal. The order–disorder transition in $LiFe_5O_8$ has been studied by TEM [16, 23] and by *in situ* high-voltage TEM [24]. A similar ordering behaviour occurs in maghemite (γ-Fe_2O_3) where the roles of iron ions and cation vacancies appear to parallel those of iron and lithium ions in lithium ferrite [25].

Present address: Department of Materials, Queen Mary College, London E1 4NS, UK.

0022–2461/87 $03.00 + .12

It has been suggested [12, 14, 26] that pre-precipitation ordering of cation vacancies can occur in non-stoichiometric Mn–Zn ferrites containing excess oxygen (so that compositions lie close to the haematite phase field). This parallels the case of oxygen-excess magnetite ($Fe_{3-x}O_4$) for which cation vacancy ordering has been conclusively proved [27]. Non-stoichiometric Mn–Zn ferrite can be envisaged as a solid solution of a stoichiometric component and a non-stoichiometric one, maghemite (γ-Fe_2O_3):

stoichiometric component

$$[(Mn, Zn)Fe_2O_4]_{1-x}$$

+

non-stoichiometric component

$$[(Fe, Mn)_{8/3}(V_{Oct} - V_{Tet})_{1/3}O_4]_x$$

where V_{Oct} = octahedral vacancy and V_{Tet} = tetrahedral vacancy. Maghemite has a cubic defective-spinel structure, in which 11% of the total cation sites that are occupied in the stoichiometric ferrite are vacant.

The equilibria of Mn–Zn ferrites with compositions of commercial interest as a function of oxygen partial pressure are known [4, 28]. Oxidation beyond the single-phase field causes precipitation of the rhombohedral phase, haematite (α-Fe_2O_3). This forms as laths in the host phase [29] which have the following crystallographic relationship [30]:

$$\{1\,1\,1\}_F \parallel (0\,0\,0\,1)_H$$

$$\langle\bar{1}\,1\,0\rangle_F \parallel \langle\bar{1}\,0\,1\,0\rangle_H$$

where F = ferrite and H = haematite.

A study of cobalt-doped (Ni, Zn)Fe_2O_4 showed that oxidation below 550° C produced no precipitation whereas grain-boundary precipitation occurred above 550° C, together with high-densities of dislocations, stacking faults and voids [31]. Different types of second phase may appear in ferrites with more than two cationic species when they are subjected to highly oxidizing conditions.

The effects of second-phase homogeneous and grain-boundary precipitation on the magnetic properties of ferrites have been considered by Bongers *et al.* [32], Mishra and Thomas [19] and Lin *et al.* [20]. Grain-boundary segregation of second phase as a consequence of the use of processing additives has also been reported [32, 33]. The oxidation behaviour of magnesium spinel, $MgAl_2O_4$, also has relevance to cubic ferrites, on account of their structural similarities. Corundum, α-Al_2O_3, is the second phase that forms. Donlon *et al.* [34] found that the orientation relationship of the corundum to the host spinel is identical to that quoted earlier [30] for haematite and Mn–Zn ferrite. But there is evidence that precursor phases to corundum form in magnesium spinel [35] and Doukhan *et al.* [36] have considered possible descriptions of a particular tetragonal precursor phase.

2. Experimental procedure

The samples used in this study were parts of a single-crystal boule supplied by the Fuji Electrochemical Company, Japan. The composition of the boule was determined by wet chemical analysis to be 55.1 mol % Fe_2O_3 (assuming all the iron to be in the form Fe^{3+}), 27.94 mol % MnO and 16.96 mol % ZnO. The Fe^{2+} content, measured by a coulometric titration technique [37], was 1.85 wt %. A weight and charge balance calculation [3] enabled the vacancy content (□) of the as-grown boule to be estimated, thereby determining that effectively the formula of the material was $Mn^{2+}_{0.536}Zn^{2+}_{0.326}Fe^{2+}_{0.077}Fe^{3+}_{2.040}\square_{0.020}O_4$. The lattice parameter of the as-grown crystal was found by means of X-ray diffraction to be 0.8487 nm [3].

The samples used in this investigation were initially cut in the form of rectangular bars with approximate dimensions 30 mm × 15 mm × 1.5 mm. Two of these bars were annealed at 1000 and 1100° C for 325 and 206 h, respectively, in an oxygen partial pressure, p_{O_2}, of 0.7% p_{O_2}. All of the results in this paper pertain to samples which were heat-treated at 0.7% p_{O_2}. When the heat treatment was completed, the samples were allowed to cool in the reacting atmosphere of the furnace. According to phase equilibria data [28] heat treatment at 1100 and 1000° C should produce single-phase and two-phase material respectively.

Thin sections were cut from the heat-treated samples by means of a diamond saw, parallel to selected low-index crystallographic planes, after the samples had been oriented suitably by the Laue X-ray back-reflection method. The sections were ground and carefully polished to thicknesses of less than 30 μm before fixing them with epoxy cement to "washer-type" electron microscope grids and ion-thinning them with 6 kV argon ions. Experience showed that unless the initial surfaces were well prepared and free from scratches, the finished ion-thinned samples were very rough, making TEM examination difficult. Ion-thinning was completed using argon ions accelerated to a lower voltage (typically 5 kV) and an angle of incidence of 11°. By this means the surface relief produced by ion-beam thinning was minimized. Ion-beam damage of the surface layers could not, however, be prevented. (This is manifest as a mottled texture on a scale of about 5 nm and it is a recognized problem with ferrites and some other spinel-structured materials.)

Transmission electron microscopy was carried out with a JEOL 200-CX instrument fitted with scanning transmission (STEM) facilities and an energy-dispersive X-ray detector and Link Systems (available in the UK) fully-quantitative analysis system (EDS). SEM examination was carried out on polished sections using a Cambridge S600 instrument fitted with a Tracor Northern semi-quantitative EDS system.

3. Results

3.1. The precipitation of second phase

SEM and TEM investigations were made on sections cut parallel to the {0 1 1} plane of the rectangular bar of the ferrite heat-treated at 1000° C. The effect of this furnace treatment was to produce oxidized surface layers on the bar and laths of second phase which penetrated into the bar from the surfaces and also

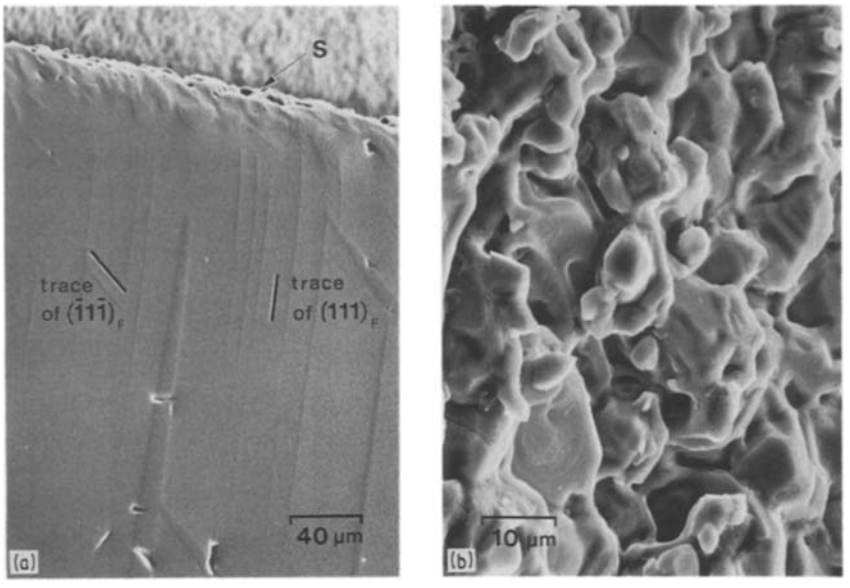

Figure 1 (a) SEM micrograph of an (0 1 1) section of ferrite heat-treated at 1000° C, showing haematite laths in the bulk and an irregular distribution of haematite nearer to the original external surface (S) of the specimen. The traces of the haematite laths are consistent with their major surfaces being parallel to the {1 1 1} planes of the ferrite. (b) SEM image of a thermally-etched surface of ferrite heat-treated at 1000° C.

occurred throughout it, as shown in Fig. 1a. The widths of the laths ranged from 0.1 μm or less, to about 20 μm. It is predominantly the nature and form of the second phase that we report here.

The presence of the second phase was readily apparent in the SEM images because it is mechanically harder than the ferrite, with the result that after polishing the specimens the second phase stands proud of the host phase. SEM/EDS X-ray microanalysis revealed that these laths contained no measurable zinc and only a small amount (< 5 wt %) of manganese, the balance being iron (oxygen not detectable). This result at once suggested that the laths were haematite. Since the orientation of the ferrite bars was known, it was straightforward to show that the laths always lay parallel to the traces of the {1 1 1} planes of the host ferrite, as demonstrated by Fig. 1a. Small voids commonly occurred in the ferrite adjacent to the interfaces between it and the largest laths. The oxidized surfaces of the bars were extremely rough as shown in Fig. 1b and consisted predominantly of haematite. The haematite surface layer penetrated to a depth of about 25 μm, as judged by transverse sections like that shown in Fig. 1a, while the laths occurred throughout the bar.

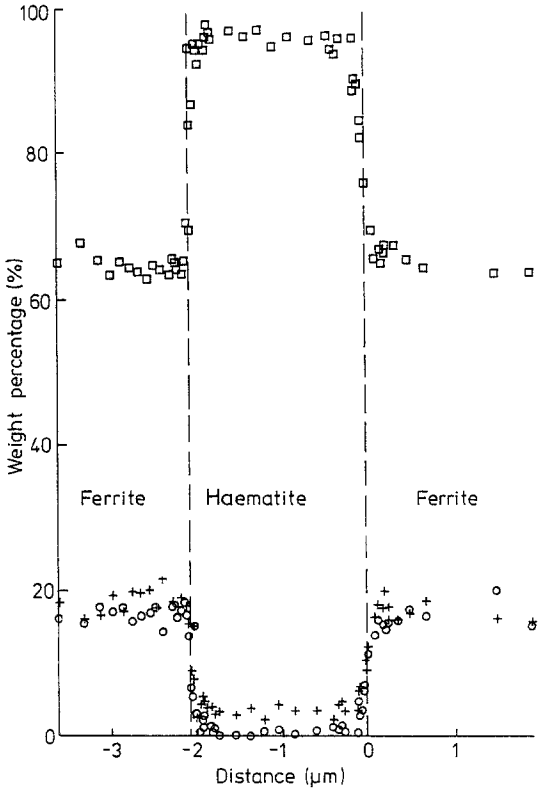

Figure 2 STEM/EDS data obtained at points along a line perpendicular to a haematite lath in ferrite heat-treated at 1000° C. The lath was oriented with its major surfaces parallel to the direction of the electron beam. (□) Iron, (+) manganese, (○) zinc.

STEM/EDS X-ray point-by-point analysis across the laths confirmed the SEM/EDS results. Fig. 2 shows a plot of the concentrations of iron, manganese and zinc transverse to a typical lath, a result which, taken with the following TEM observations, proves the laths to be essentially haematite. Fig. 3a is an image recorded with the electron beam aligned slightly off a ⟨0 1 1⟩ zone axis, a condition which produced the least strain contrast from the bending of the foil caused by the presence of the laths. The ferrite–lath interface is parallel with the beam direction and the trace of the lath is parallel to a ⟨2 1 1⟩ direction, which makes the interface a {1 1 1} plane. When a lath is oriented so that the ferrite–lath interface lies perpendicular to the direction of the electron beam, three sets of moiré fringes occur at the lath, as illustrated in Fig. 3b, since in this $\langle 1\,1\,1\rangle_F$ zone-axis orientation both host and second phase have three-fold symmetry. Fig. 3c shows the selected-area diffraction pattern corresponding to Fig. 3b. This is interpreted as the superposition of a $\langle 1\,1\,1\rangle_F$ pattern and the $[0\,0\,0\,1]_H$ pattern, with multiple electron diffraction effects. A full investigation of the crystallography revealed the relationships

$$\{1\,1\,1\}_F \parallel (0\,0\,0\,1)_H$$

$$\langle \bar{1}\,1\,0\rangle_F \parallel \langle \bar{1}\,0\,1\,0\rangle_H$$

This is the same relationship between haematite and Mn–Zn ferrite as reported by Carter *et al.* [30].

Lattice imaging methods were also applied, thereby enabling the host–lath interfaces to be studied in more

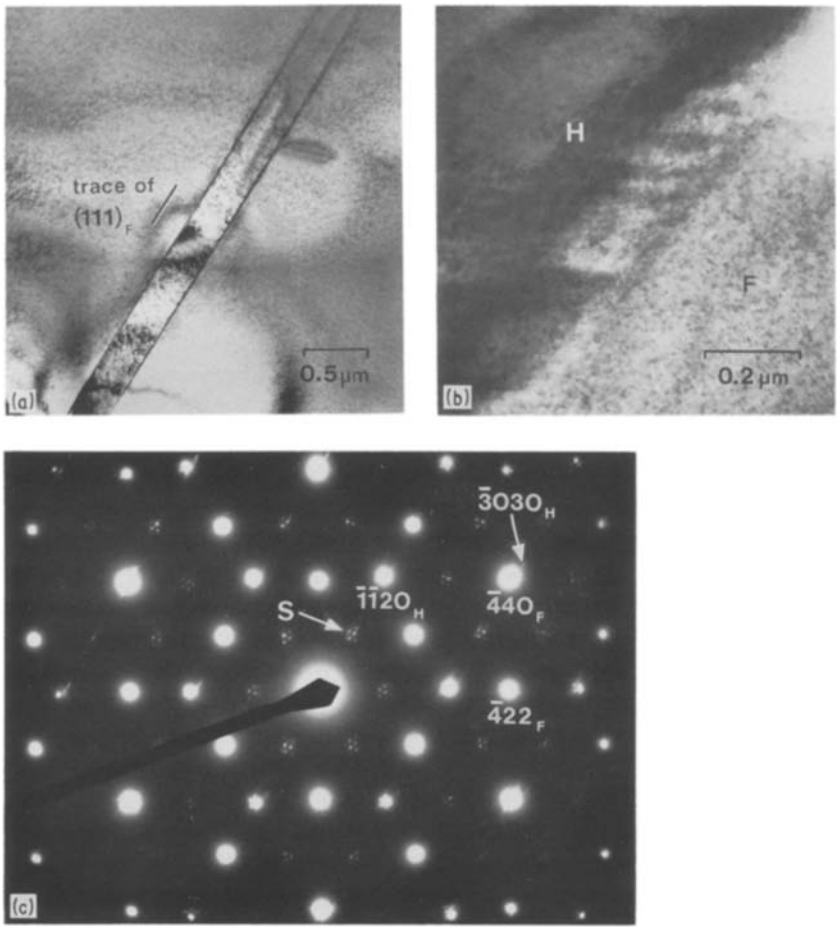

Figure 3 (a) TEM micrograph of an $\{0\,1\,1\}$ section of ferrite heat-treated at 1000° C showing a haematite lath orientated with its major surfaces almost parallel to the electron beam. The strong background contrast is caused by ion-thinning. (b) TEM micrograph of a haematite lath orientated so that its major faces are perpendicular to the electron beam. The ferrite and haematite phases overlap, producing moiré fringes. (c) Electron diffraction pattern corresponding to (b), showing the haematite $[0\,0\,0\,1]_H$ zone-axis pattern superposed on a ferrite $\langle 1\,1\,1\rangle_F$ zone-axis pattern. (S) indicates satellite spots which result from the double diffraction of electrons by both of the phases.

detail and leading to the discovery of regions of incipient second-phase precipitation. Fig. 4a is a high-resolution image with the electron beam parallel to a $\langle 1\,1\,0\rangle_F$ zone axis and also to a ferrite–haematite interface. By this means it was discovered that there was not exact parallelism between the $\langle \bar{1}\,1\,0\rangle_F$ and $\langle \bar{1}\,0\,1\,0\rangle_H$ directions. They are rotated relative to each other by $1.1 \pm 0.2°$ about an axis perpendicular to the ferrite–haematite growth plane (i.e. $[0\,0\,0\,1]_H$ and $\langle 1\,1\,1\rangle_F$). The misalignment was initially estimated from differences in the angular coordinates of the two zone axes, determined from the tilt stage of the microscope. A more accurate value was then obtained from electron diffraction patterns, using Kikuchi lines to obtain exact zone axis settings. Because the specimen in Fig. 4a was orientated with the $\langle \bar{1}\,1\,0\rangle_F$ zone axis exactly parallel to the direction of the electron beam, the $[\bar{1}\,0\,1\,0]_H$ direction was inclined at an angle of

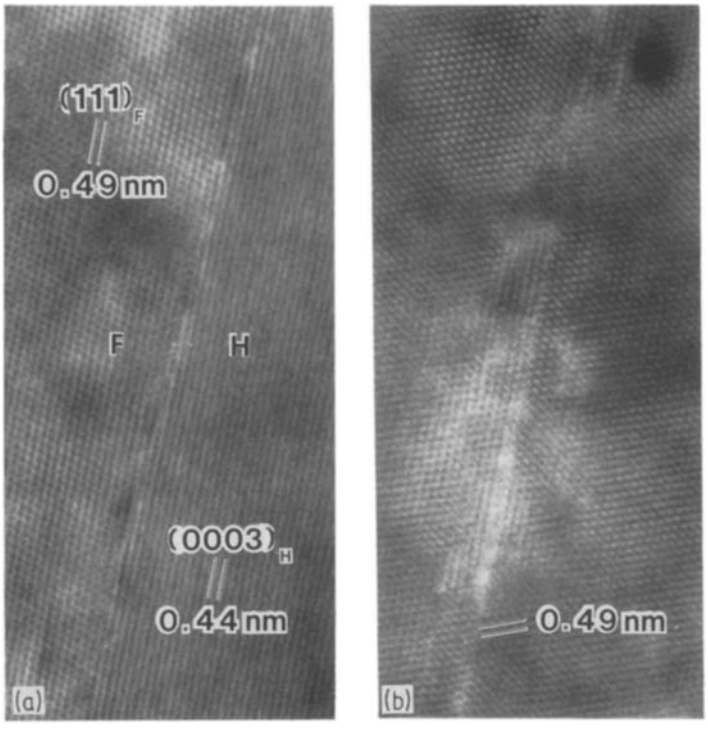

Figure 4 (a) $\langle \bar{1}\,1\,0\rangle_F$ zone-axis lattice image recorded in the region of an interface between the ferrite host and a lath of haematite. The $(0\,0\,0\,3)_H$ lattice planes are resolved. (b) $\langle 1\,1\,0\rangle_F$ zone-axis lattice image of a narrow band of distorted lattice in ferrite heat-treated at 1000° C.

1.1 $\pm$ 0.2° to the beam. This explains why the $(1\bar{2}10)$ planes of the haematite are not seen, even though their spacing (0.251 nm) is greater than the resolution of the 200-CX microscope. Analysis of the electron diffraction patterns from a number of ferrite–haematite contacts confirmed both the details of the results obtained from high-resolution EM images and the universality of the relationship.

SEM and TEM investigations of the sample which was heat-treated at 1100° C showed it to be completely free of second-phase precipitates.

3.2. Incipient precipitation

High-resolution imaging further revealed that there occurred in the two-phase material (i.e. heat-treated at 1000° C) straight, narrow (< 5 nm) bands, parallel to $\{1\,1\,1\}_F$ planes, which could not be attributed to the presence of true precipitates, but which showed the ferrite lattice to be strained locally and possibly to indicate changes in the concentration of cations. Fig. 4b illustrates these points. It is unwise to draw any far-reaching conclusions from lattice images without making comparisons with computer-simulated images. However, it is at least apparent that the image in Fig. 4b shows inhomogeneities on the $\{1\,1\,1\}_F$ planes, and these might well take the form of layers rich in one cation species. The disposition and orientation of these lattice-distorted bands in the oxidized ferrite leads us to suggest that they are sites of incipient haematite nucleation, especially since similar defects were not observed in the material having a lower oxygen content (heat-treated at 1100° C).

In the course of lattice imaging to study second-phase precipitation effects it was also found that there were planar defects in the ferrite lying parallel to $\{1\,1\,0\}_F$ planes. Some of these defects are imaged in Fig. 5 (e.g. at A and B). Although the pairing of some of these faults gives the regions between them the superficial appearance of microtwins, spinel-structured oxides normally twin on $\{1\,1\,1\}$ planes (e.g. see Hornstra [38]). Moreover, no twin reflections could be found in the diffraction patterns and there was no significant change in the diffraction contract across the defects. These defects offset the $\{1\,1\,1\}_F$ planes. The termination of defects at partial dislocations is indicted at C and D (Fig. 5), while a single, unpaired fault occurs at G.

Investigation showed these faults to be conservative antiphase boundaries (APBs), i.e. the displacement vector lay in the plane of the defect. The displacement vector could not be determined unequivocally because of the small size of the defects (typically between 0.02 and 0.1 μm in length). However, the shortest vector which would produce the relative displacements of the $\{1\,1\,1\}_F$ planes seen in Fig. 5, and therefore the one most likely to be energetically favoured, is $(a/2)\langle 0\,0\,1\rangle$. Because the displacement vector is in the plane of the defect it can also be envisaged as a shear vector. Close to the APBs there occurred other planar defects which gave only a slight mismatch of the $\{1\,1\,1\}_F$ planes adjacent to them (e.g. at E and F in Fig. 5). The relationship between these two types of defect is not completely determined. But because similar features were not found in the ferrite with the lower oxygen content, we take the view that they are intimately related to the non-stoichiometry of the material and we discuss their nature at a later point.

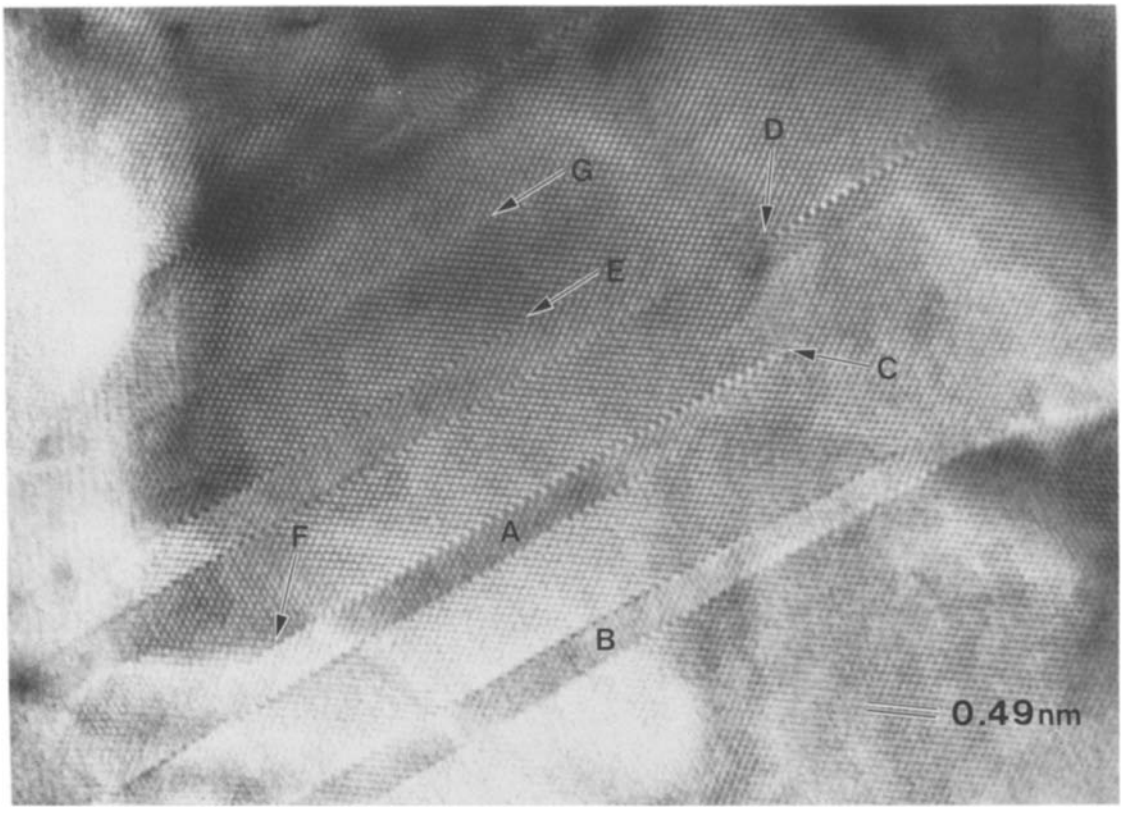

Figure 5 $\langle 0\,1\,1\rangle_F$ zone-axis lattice image of planar defects parallel to an $\{0\,1\,1\}_F$ plane in ferrite heat-treated at 1000° C. The defects, two of which terminate at the positions marked C and D, are conservative APBs. Other defects, for example at positions marked E and F, correspond to an offset of the imaged lattice planes crossing the defect which is not a simple fraction of a lattice vector.

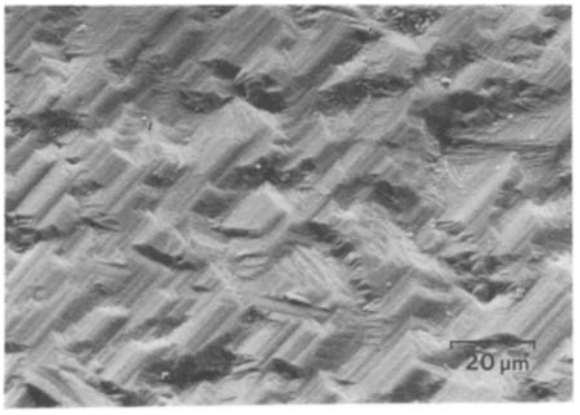

Figure 6 SEM micrograph of a thermally etched {1 1 0} surface of a ferrite specimen heat-treated at 1100° C.

3.3. Inhomogeneous ferrite material

3.3.1. Zinc-deposited surface zones

It is possible, by using an appropriate heat treatment, to produce on all specimens of ferrite a zone at the external surface that does not have the bulk composition and yet is free from haematite. Fig. 6 shows the {0 1 1} surface of a specimen that was annealed for 206 h at 1100° C. It is thermally etched and also zinc-deficient (with respect to the initial composition of the ferrite) because of the loss of this volatile element from external surfaces at high temperatures. SEM/EDS investigation of a polished section cut perpendicular to the surface of the specimen did not reveal the presence of any second phase, but showed that the zinc deficiency was detectable to depths of about 200 μm, as illustrated by the results reproduced in Fig. 7.

The composition of a surface region in a specimen heat-treated at 1000° C for 325 h was also investigated by SEM/EDS. There was no appreciable surface depletion of zinc (< 1% variation in the concentration with respect to that of the bulk) in the ferrite phase closest to the haematite-rich surface layer. This absence of zinc depletion in the ferrite layer just underneath the surface layer suggests that the haematite presents an effective barrier to the diffusion of zinc, thereby preventing its loss by volatilization at the free surfaces.

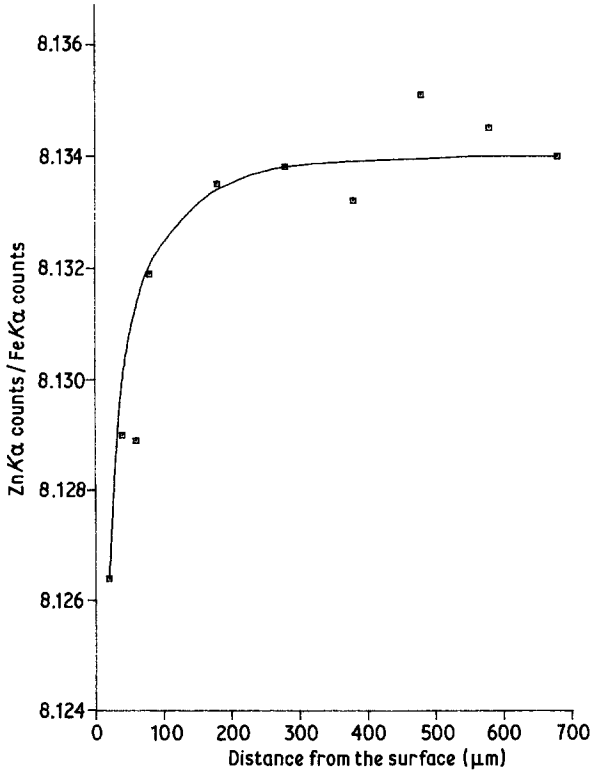

Figure 7 The ratio of counts ZnKα/FeKα, determined by means of SEM/EDS microanalysis, as a function of distance from the exterior surface of ferrite heat-treated at 1000° C.

3.3.2. Zinc-depleted interior regions

Interior regions which were more susceptible to charging under the electron beam than normal ferrite were found in the sample heat-treated at 1000° C. STEM/EDS analysis of these regions showed them to be depleted in zinc. One such region is shown in Fig. 8a, and averaging several analyses of it gave the following results: Fe 76.(2) ± 1.5 wt %, Mn 21.(4) ± 1.4 wt %, Zn 2.(4) ± 1.0 wt % (errors are standard deviations). It was noticed that these somewhat rare, zinc-depleted, beam-charging areas sometimes also showed the presence of small plate-like precipitates, which are visible in Fig. 8a and shown under different imaging conditions in Fig. 8b. These figures indicate that the precipitates are coherent with the host ferrite, because of the moiré patterns that occur. The diffraction patterns from this and similar areas exhibit "splitting" of higher-order reflections, visible in Fig. 8c, as a result of there being two coherent phases with slightly different lattice parameters. Measurement of the patterns established that the second-phase platelets were spinel-structured and had a lattice parameter that was 4.0 ± 0.1% larger than that of the ferrite (i.e. for the platelets a_0 = 0.91 ± 0.02 nm). The platelets had a {0 1 1} growth habit and were observed in ion-thinned sections which had a {0 1 1} surface orientation. This suggested that they might only occur at the surface of the specimens, a fact which was soon confirmed using stereoscopic imaging methods.

A probable explanation for the occurrence of the platelets only near to the surfaces relates to the ion-beam thinning method that was used to prepare the TEM specimens. The similarity of the platelets to Guinier–Preston zones [39, 40] prompts the thought that they are rich in at least one cation species (a consequence of being depleted in the most volatile element, zinc). Localized preferential loss of zinc is likely to occur if the developing surface topography causes incident ions to be deflected and concentrated into certain regions as a result of surface charging.

3.3.3 Iron-rich regions

Despite the high quality of the original crystal boule and the anticipated chemical homogeneity of the samples prior to heat treatment, some evidence was found for internal compositional inhomogeneities (in addition to the precipitation and incipient precipitation features already described) on a somewhat larger scale. One such area was observed by TEM in a thinned specimen taken from the sample heat-treated at 1000° C for 325 h. Although electron diffraction showed the region to be spinel-structured (a_0 = 0.85 ± 0.02 nm), it was different in composition

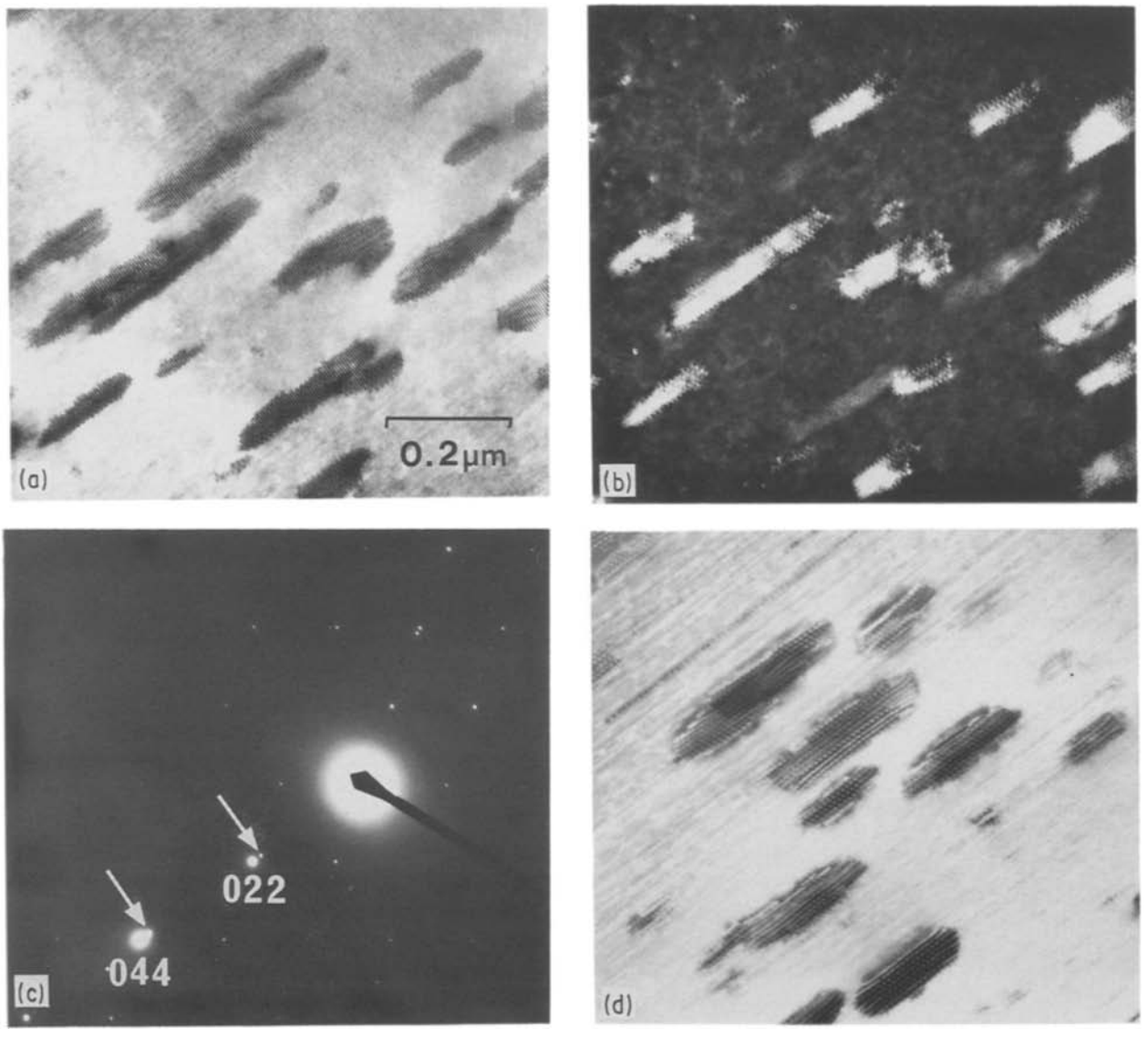

Figure 8 Corresponding (a) bright-field and (b) dark-field images of a zinc-depleted region in an {0 1 1} section of ferrite heat-treated at 1000° C. The presence of precipitates of a second phase which is spinel-structured and coherent with the host ferrite is indicated by the moiré patterns. (c) Diffraction pattern showing excitation of the 0 2 2 systematic row. Reflections caused by the particles of second phase are indicated by arrows and their positions show that the lattice parameter of the second phase is 4.0 ± 0.1% greater than that of the host phase. (d) An image of a zinc-depleted region, formed with the electron beam parallel to an ⟨0 1 1⟩ zone axis and multiple reflections operating.

from the bulk of the surrounding ferrite, being iron-rich. The averaged results of STEM/EDS analyses of the region were as follows: Fe 94.(4) ± 1.2 wt %, Mn 3.(7) ± 0.5 wt %, Zn 1.(9) ± 0.3 wt % (the errors are standard deviations). The region exhibited a number of interesting features, the most immediately obvious being a high density of subgrain boundaries illustrated in Fig. 9a, which tended to be aligned parallel with {0 1 1} planes.

Another property which distinguished this iron-rich region from the normal ferrite was a high susceptibility to charging when irradiated with the electron beam (all specimens were given a thin coating of amorphous carbon in order to avoid charging problems and, in general, this was effective). Dislocation loops formed within two minutes' exposure to the electron beam, and after about 40 min irradiation the damage was extensive, as shown by Fig. 9b. Because of the large elastic strains associated with the loops, it was found that the best ways of imaging them was by dark-field (DF) or weak beam dark field (WBDF) methods. By using trace analysis and diffraction contrast techniques, it was established that the loops were pure edge in character, with a Burgers vector $\boldsymbol{b} = (a/4)\langle 0\,1\,1\rangle$. This is illustrated by Figs 9c and d, which also show that double loops are destroyed as irradiation proceeds.

An excess of iron in the ferrite (with respect to the stoichiometric concentration for the same equilibrium temperature) implies an increase in the concentration of cation vacancies [28]. We believe that the role of the electron irradiation during the above observations was to aggregate pre-existing point defects in a highly cation-deficient phase. The iron-rich region was probably a maghemite-like phase, but we did not observe diffraction spots consistent with a maghemite structure. However, it is possible that our electron diffraction patterns were not recorded at a sufficiently early stage of the alteration process to show strong reflections normally associated with a maghemite structure, and that the bulk of the highly defective maghemite-like phase transforms to a true spinal structure very rapidly.

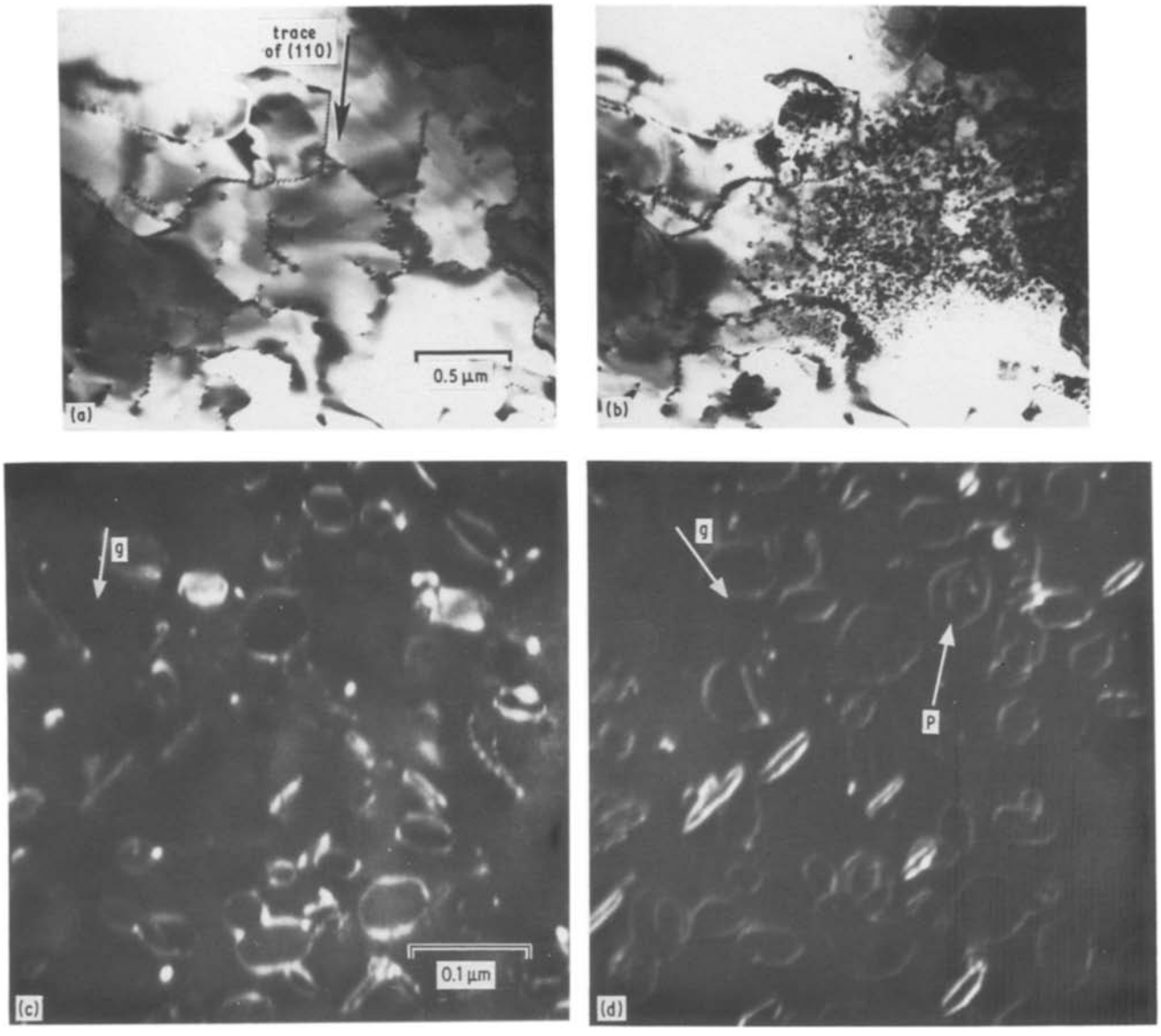

Figure 9 Region with many tilt subgrain boundaries in ferrite heat-treated at 1000° C. (a) Bright-field (BF) image recorded with the electron beam aligned close to an ⟨0 0 1⟩ zone axis. The sub-boundaries tend to be aligned with {0 1 1} planes. (b) BF image showing the same general area after 40 min exposure to the electron beam, which produced extensive radiation damage. (c, d) Dark-field images taken in the region of images (a) and (b) after approximately 40 min irradiation. The images were recorded with the beam close to an ⟨0 0 1⟩ zone axis, using (c) diffraction vector $\mathbf{g} = 0\,4\,0$ and (d) $\mathbf{g} = 4\,4\,0$. After 40 min irradiation no whole double loops remained, but some residual loop segments are visible at P.

4. Discussion

The morphology that we have observed for the haematite laths is similar to that previously reported by Ozawa *et al.* [29]. The fact that the haematite occurs as fairly coarse laths penetrating into the bulk and not as a fine-scale phase, distributed homogeneously at a given depth from the surface, invites some comment. We appear to be dealing with a case of heterogeneous nucleation, but this does not exclude the possibility that the morphology of the haematite second phase is of some significance. The nucleation process will occur at external surfaces without great difficulty, since relatively gross defects will usually exist to promote bond-breaking. The form of the laths might be related to growth along crystal defects (either pre-existing or nucleation-induced) or because the presence of an embryo second phase offers an easy diffusion path for further growth, either in the haematite itself or in adjacent zones.

The data of Reddy and Cooper [41] shows that the oxygen diffusion coefficient for single-crystal haematite at 1000° C is about an order of magnitude less than that estimated for single-crystal ferrite at the same temperature by extrapolating the data of Castle and Surman [42] on magnetite. Since the oxygen ion is the slowest moving species in spinel-structured oxides [43, 46] and therefore rate-controlling, the possibility of an easy diffusion path within the haematite is discounted. However, there is reason to think that oxygen diffusion in the proximity of the haematite may be enhanced. Ando and Oishi [45] showed that the rate of self-diffusion of oxygen in monocrystalline Mg-spinel in which corundum has precipitated is significantly higher than the rate found in single-phase Mg-spinel [46]. The higher diffusivity in the two-phase material was attributed to enhancement as a result of the disordered structure of the phase boundaries. This behaviour, which we assume is relevant to ferrite, could

explain the coarsening of existing laths in preference to further nucleation and could also explain the form of haematite advancement into the bulk ferrite.

Our TEM work has confirmed the basic epitaxial relationship between haematite and Mn–Zn ferrite previously reported by Carter *et al.* [30] following an X-ray diffraction investigation of large grains in polycrystals. However, the TEM study shows that the crystallographic relationship is not adhered to precisely. There is a rotation of the $(0\,0\,0\,1)_H$ growth plane by $1.1 \pm 0.2°$ relative to the conjoining $\{1\,1\,1\}_F$ plane. The rotation produces an angular deviation between the $\langle\bar{1}\,1\,0\rangle_F$ and $\langle\bar{1}\,0\,1\,0\rangle_H$ directions of $1.1 \pm 0.2°$. It is interesting that Carter *et al.* [30] mention a 2° spread in the orientation relationship which they determined by X-ray methods. They may have been seeing the effect which we report here.

We have considered the observed small deviation from exact epitaxy in terms of simple models for the best fit of the adjacent anion planes of ferrite and haematite, but such methods are neither adequate in terms of the physical situation, nor particularly revealing. It appears that an explanation for the misorientation across the interface will only emerge from fairly sophisticated computations which look at both anion and cation positions close to the interface in order to minimize the interaction energies.

Haematite has a rhombohedral structure (space group $R\bar{3}c$) and there are hexagonal close-packed arrays of oxygen ions parallel to the basal plane $(0\,0\,0\,1)_H$, with Fe^{3+} ions arranged in two-thirds of the octahedral sites [44]. The $\{1\,1\,1\}$ planes of the spinel-structured Mn–Zn ferrite also have hexagonal close-packed arrays of oxygen ions and these are separated by alternating, differing layers of cations. In one layer the cations occupy one-quarter of the octahedral sites and one-quarter of the tetrahedral sites. Cations in the other type of layer form a Kagome structure [47] and occupy three-quarters of the octahedral sites [38]. The separations of the oxygen ions in the close-packed layers of the haematite and ferrite phases are 0.291 and 0.300 nm, respectively, giving a disregistry of only 3% at room temperature. Thermal expansion data for haematite [48] and for some ferrites [49] suggest that the mismatch will be reduced to about 2.7% at 1000° C.

The mismatch between the oxygen ion separations is likely to be the reason for the observed relative rotation between the two phases at the epitactic interfaces. The cations are small compared with the anions and, in general, the close packing of the latter will normally be the major factor in determining the structure of grain boundaries and phase boundaries. The observed rotation at the ferrite–haematite interface must be such as to give a minimum-energy arrangement. However, the rotation is likely to be a function of ferrite composition since this will affect the lattice parameter of the ferrite and, to a lesser extent presumably, the composition and lattice parameters of the precipitating haematite phase.

We believe that we have observed two different types of planar defect in the ferrite which are related to local non-stoichiometry and probably signify incipient precipitation of a second phase. These defects are visible in lattice images of the ferrite which was heat-treated at 1000° C. The narrow bands of distorted lattice parallel to the $\{1\,1\,1\}_F$ planes are not amenable to microanalysis but they are probably iron-rich and their number density and orientation are consistent with their being precursors to the appearance of discrete haematite laths. The other type of defect observed has the characteristics of a conservative APB, giving a fault in the stacking of cations in relation to the spinel structure, but leaving the oxygen sublattice undisturbed. A possible mechanism for the creation of such defects would be pre-precipitation ordering of cation vacancies on $\{1\,1\,0\}$ planes, followed by a shear on the plane to eliminate highly unfavourable electrostatic interactions. Although this would involve the clustering of initially-charged point defects, it may lead to the stabilization of the relatively defect-laden ferrite phase during oxidation (initial cation vacancy concentration > 0.9% of all cation sites) by means of an overall reduction in lattice free energy, as occurs in oxygen-excess wustite, $Fe_{1-x}O$ [50]. One manner in which this might be accomplished is envisaged to be as follows.

Individual cation vacancies are negatively charged and so a local rearrangement of the ions in a vacancy-rich region can be made to reduce the electrostatic contribution to the free energy. A shear of the stoichiometric spinel structure on the $\{1\,1\,0\}$ planes by an amount $(a/2)\langle 0\,0\,1\rangle$ would, however, be highly unfavourable since it would reduce the shortest distance across the resulting fault between octahedral and tetrahedral sites from $0.41a_0$ to $0.22a_0$ (where a_0 is the lattice parameter). But the presence of a cation vacancy at either of these sites would make such a $\frac{1}{2}\langle 0\,0\,1\rangle$ shear fault more energetically favoured. The tetrahedral–tetrahedral and octahedral–octahedral cation–cation shortest distances are not affected by such a fault, and the positions of the octahedral cations relative to their nearest octahedral neighbours are unchanged. The nearest-neighbour tetrahedral cations across the plane of the fault would have an oxygen ion directly between them, however – a situation not found in the perfect structure. This configuration would appear to be energetically favourable, since the oxygen ion would shield the cations from each other. If the $\{1\,1\,0\}$ defects that we have observed are indeed an indication and consequence of vacancy ordering, this would be the only reported case of such behaviour in Mn–Zn ferrite. However, the occurrence of precipitation ordering in this material has been suggested by Gallagher *et al.* [12] and by Hoekstra *et al.* [26] on the basis of magnetic permeability data, and Kosinski *et al.* [14] as a means of interpreting measurements of fracture toughness. The model which we have advanced here has some points of similarity with that of Doukhan *et al.* [36] which interpreted precipitates in non-stoichiometric Mg-spinel in terms of a periodic crystallographic shear on $\{1\,0\,0\}$ planes plus additional ordered cation vacancies.

Acknowledgements

We thank S. L. Callahan, R. E. Tressler and D. W.

Johnson Jr for supplying us with ferrite samples and A. Alexander for carrying out some heat treatments under controlled p_{O_2} conditions. We gratefully acknowledge support from the Science and Engineering Research Council in the form of a studentship (M.J.R.) and research grant GR/C/29072.

References

1. R. D. FISHER and J. D. BLADES, *IEEE Trans. Magn.* **MAG-13** (1971) 350.
2. H. YOKOYAMA, Y. TAKEOKA, M. ISSIKI, S. TAKEI and Y. HIROSE, in Proceedings of 3rd International Conference on Ferrites, 1980, Kyoto, Japan, edited by H. Watanabe, S. Iida and M. Sugimoto (Centre for Academic Publications, Tokyo, 1981) p. 679.
3. S. L. CALLAHAN, R. E. TRESSLER, D. W. JOHNSON and M. J. REECE, in "Deformation of Ceramics II", edited by R. C. Bradt and R. E. Tressler (Plenum, New York, 1984) p. 177.
4. P. SLICK, in Proceedings of 2nd International Conference on Ferrites, 1970, Kyoto, Japan, edited by Y. Hoshino, S. Iida and M. Sugimoto (University of Tokyo Press, Tokyo, 1971) p. 81.
5. TH. J. BERBEN, D. J. PERDUIJN and J. P. M. DAMEN, in Proceedings of 3rd International Conference on Ferrites, 1980, Kyoto, Japan, edited by H. Watanabe, S. Iida and M. Sugimoto (Centre for Academic Publications, Tokyo, 1981) p. 722.
6. N. N. GREENWOOD, "Ionic Crystals, Lattice Defects and Non-stoichiometry" (Butterworths, London, 1968) p. 194.
7. G. D. PRICE, S. L. PRICE and J. K. BURDETT, *Phys. Chem. Minerals* **8** (1982) 69.
8. M. PAULUS and F. REVERCHON, *J. Phys. Radium* **22** (1961) (8) Suppl. 6, 103A.
9. R. MORINEAU, *Phys. Status Solidi (a)* **38** (1976) 559.
10. B. GILLOT and F. JEMMALI, *ibid.* **76** (1983) 601.
11. K. OHTA, *J. Phys. Soc. Jpn* **18** (1963) 685.
12. P. K. GALLAGHER, E. M. GYORGY and D. W. JOHNSON, *Amer. Ceram. Soc. Bull.* **57** (1978) 812.
13. T. TANAKA, *Jpn. J. Appl. Phys.* **14** (1975) 1897.
14. S. G. KOSINSKI, S. VAIDYA, D. W. JOHNSON and R. E. TRESSLER, *Amer. Ceram. Soc. Bull.* **58** (1979) 616.
15. G. S. BAKER and M. J. WHELAN, in Proceedings of 7th International Congress on Electron Microscopy, Vol. 2, edited by P. Farand (Société Francais de Microscopie Electronique, Paris, 1970) p. 283.
16. O. VAN DER BIEST and G. THOMAS, *Phys. Status. Solidi (a)* **24** (1974) 65.
17. P. VEYSSIERE, J. RABIER and J. GRILKE, *ibid.* **31** (1975) 605.
18. P. VEYSSIERE, J. RABIER, H. GAREM and J. GRILKE, *Phil. Mag.* **33** (1976) 143.
19. R. K. MISHRA and G. THOMAS, in Proceedings of 3rd International Conference on Ferrites, 1980, Kyoto, Japan, edited by H. Watanabe, S. Iida and M. Sugimoto (Centre for Academic Publications, Tokyo, 1981) p. 257.
20. I.-N. LIN, R. K. MISHRA and G. THOMAS, *IEEE Trans. Magn.* **MAG-20** (1984) 134.
21. R. K. MISHRA, PhD thesis, University of California (1977).
22. R. K. MISHRA, O. VAN DER BIEST and G. THOMAS, *J. Amer. Ceram. Soc.* **61** (1978) 121.
23. S. LEFEBVRE, R. PORTIER and M. FAYARD, *Phys. Status Solidi* **24**(a) (1974) 79.
24. O. VAN DER BIEST, E. P. BUTLER and G. THOMAS, in Proceedings of 26th Electron Microscopy Society of America (Claitors, Baton Rouge, USA, 1975) p. 26.
25. P. P. K. SMITH, *Contrib. Mineral. Petrol.* **69** (1979) 249.
26. B. HOEKSTRA, E. M. GYORGY, P. K. GALLAGHER, D. W. JOHNSON, G. ZYDZIK and L. G. VAN UITERT, *J. Appl. Phys.* **49** (1978) 4902.
27. D. H. LINDSLEY, in "Oxide Materials, Short Course Notes", Vol. 3, edited by D. Rumble (Mineralogy Society of America, Washington, DC, 1976) p. L-12.
28. R. MORINEAU and M. PAULUS, *Phys. Status Solidi (a)* **20** (1973) 373.
29. K. OZAWA, S. KITAMURA and S. TAKAHASHI, in Proceedings of 2nd International Conference on Ferrites, 1970, Kyoto, Japan, edited by Y. Hoshino, S. Iida and M. Sugimoto (University of Tokyo Press, Tokyo, 1971) p. 332.
30. R. E. CARTER, W. L. ROTH and C. A. JULIEN, *J. Amer. Ceram. Soc.* **42** (1959) 533.
31. M. P. HARMER, R. K. MISHRA and G. THOMAS, *Commun. Amer. Ceram. Soc.* **66** (1983) C-44.
32. P. F. BONGERS, F. J. A. DEN BROEDER, J. P. M. DAMEN, P. E. C. FRANKEN and W. T. STACY, in Proceedings of 3rd International Conference on Ferrites, 1980, Kyoto, Japan, edited by H. Watanabe, S. Iida and M. Sugimoto (Centre for Academic Publications, Tokyo, 1981) p. 265.
33. I.-N. LIN, R. K. MISHRA and G. THOMAS, in Proceedings of Conference on Advances in Materials Characterization, edited by D. R. Rossington, R. A. Condrate and R. L. Snyder (Plenum, New York, 1983) p. 351.
34. W. T. DONLON, T. E. MITCHELL and A. H. HEUER, *J. Mater. Sci.* **17** (1982) 1389.
35. M. H. LEWIS, *Phil. Mag.* **20** (1969) 985.
36. N. DOUKHAN, J. C. DOUKHAN and B. ESCAIG, *Mater. Res. Bull.* **11** (1976) 125.
37. P. K. GALLAGHER, *Amer. Ceram. Soc. Bull.* **57** (1978) 576.
38. J. HORNSTRA, *J. Phys. Chem. Solids* **15** (1960) 311.
39. A. GUINIER, *Nature* **142** (1938) 569.
40. G. D. PRESTON, *Nature* **142** (1938) 570.
41. K. P. R. REDDY and A. R. COOPER, *J. Amer. Ceram. Soc.* **66** (1983) 664.
42. J. E. CASTLE and P. L. SURMAN, *J. Phys. Chem.* **71** (1967) 4255.
43. W. D. KINGERY, D. C. HILL and R. P. NELSON, *J. Amer. Ceram. Soc.* **43** (1960) 473.
44. A. F. WELLS, "Structural Inorganic Chemistry" (Oxford University Press, Oxford, 1984).
45. K. ANDO and Y. OISHI, *J. Ceram. Soc. Jpn* **83** (1975) 417.
46. *Idem, J. Chem. Phys.* **61** (1974) 625.
47. S. IIDA, *J. Phys. Soc. Jpn* **12** (1957) 222.
48. B. T. M. WILLIS and H. P. ROOKSBY, *Proc. Phys. Soc. (Lond.)* **66B** (1952) 950.
49. W. R. BUESSEM and A. DORF, in Proceedings of Metal Powder Association, 13th Annual Meeting, Chicago, 1957, Vol. 2, p. 196.
50. C. R. A. CATLOW and B. E. F. FENDER, *J. Phys. C.* **8** (1975) 3267.

Received 5 August
and accepted 22 September 1986